Surface & Coatings Technology 473 (2023) 129982

Contents lists available at ScienceDirect

Surface & Coatings Technology

journal homepage: www.elsevier.com/locate/surfcoat

Full Length Article

Electrolyte exposure time effects on structure, composition and biocompatibility of microarc oxidation coatings on Mg-Ca-Zn alloys

Ekaterina S. Marchenko [a], Arina A. Shishelova [a], Pavel I. Butyagin [a], Ivan I. Gordienko [b], Anton P. Khrustalev [c], Svetlana S. Arbuzova [a], Ilya A. Zhukov [c], Gulsharat A. Baigonakova [a,*], Alex A. Volinsky [a,d,**]

[a] Laboratory of Superelastic Biointerfaces, National Research Tomsk State University, 36 Lenin Ave., 634045 Tomsk, Russia
[b] Department of Pediatric Surgery, Ural State Medical University, 620014 Yekaterinburg, Russia
[c] Laboratory of Metallurgy Nanotechnologies, National Research Tomsk State University, 36 Lenin Ave., 634045 Tomsk, Russia
[d] Department of Mechanical Engineering, 4202 E. Fowler Ave. ENG030, University of South Florida, Tampa, FL 33620, USA

ARTICLE INFO

Keywords:
Magnesium alloys
Coating
Micro-arc oxidation
Structure
Biodegradation
Biocompatibility

ABSTRACT

The problem of using magnesium in medicine is biodegradation, which leads to the loss of the implant mechanical integrity before the bone tissue formation. Doping and subsequent coating deposition is an effective solution to this problem. This paper investigates the effects of electrolyte exposure time during micro-arc oxidation of the Mg-Ca-Zn alloy on its phase composition, biodegradation, and biocompatibility. As a result of micro-arc oxidation, a dense coating with a gradient structure is formed on the surface of the Mg-Ca-Zn alloy, consisting of amorphous and amorphous-nanocrystalline parts. The amorphous layers of the coating mainly consist of O, P, and Mg. The nanocrystalline layer is enriched in F, while the diffusion zone is enriched in O, F, and Mg. The coating has a porous structure typical for microarc oxidation. The nonlinear behavior of the diffraction pattern at small diffraction angles indicates the amorphous state of the coating. The amount of amorphous component is increasing with exposure time, indicating an increase in the coating thickness. Scratch testing with a diamond indenter tip indicates good coating adhesion. All coated Mg-Ca-Zn samples show a significant reduction in weight loss compared to the uncoated sample after 21 days in the culture medium. Surgical treatment of rabbit femurs with implants made from coated Mg-Ca-Zn samples demonstrated high biocompatibility. Clinical evaluation of the results showed a complete absence of purulent-inflammatory complications in all animals during the first 28 days after implantation.

1. Introduction

Magnesium and its alloys are widely used as biodegradable bone implants and stents since they exhibit good biocompatibility, physical and mechanical properties, including high strength and low Young's modulus [1,2]. The main problem of magnesium alloys use in medicine is the high biodegradation rate in the aggressive environment of the body, which leads to intensed release of hydrogen gas. Also, a high degree of biodegradation and low corrosion resistance of magnesium alloys leads to the loss of implant mechanical integrity until the formation of new bone tissue. Therefore, magnesium implants must have high mechanical strength at the early stages of healing for strong fixation of bone tissue [3,4]. Alloying is one of the methods for controlling corrosion and improving the mechanical properties of Mg alloys. It is important that the main components of a biodegradable material are metabolized in the human body without the formation of toxins [5]. Rare earth metals doping of magnesium alloys increases the yield strength to more than 450 MPa, yet these elements are toxic to the body when released during implant biodegradation [6,7]. The addition of Al and Mn increases Mg alloys' mechanical properties through grain refinement, and also improves corrosion resistance. However, Al and Mn are considered neurotoxic. The addition of Li increases Mg alloys' ductility, but can cause defects in the cardiovascular system. The safest alloying elements of magnesium alloys include Zn, Ca, Sr, Zr, and can also improve mechanical and corrosion properties [8–10]. The Mg-Ca-Zn system is a promising alloy for orthopedic applications. Mg-Ca-Zn

* Corresponding author.
** Correspondence to: Department of Mechanical Engineering, 4202 E. Fowler Ave. ENG030, University of South Florida, Tampa, FL 33620, USA.
E-mail addresses: baigonakova@mail.tsu.ru (G.A. Baigonakova), volinsky@usf.edu (A.A. Volinsky).

https://doi.org/10.1016/j.surfcoat.2023.129982
Received 27 June 2023; Received in revised form 23 August 2023; Accepted 31 August 2023
Available online 1 September 2023

alloys can be easily deformed and machined, and also have low density, which increases their prospects for manufacturing implants [11–16]. An optimal Zn concentration of up to 4 wt%, and Ca up to 1 wt% was established to improve Mg alloys' properties [16–18]. However, alloying does not solve the biodegradation problem.

An effective way to improve the magnesium alloys' biodegradation is to modify the surface by applying coatings. Coating magnesium alloys is possible by electrochemical or chemical deposition, microarc oxidation, vapor phase deposition, ion implantation, and laser processing. Electrochemical and chemical coating methods are complicated by the need of thorough substrate surface preparation due to the high magnesium reactivity. In the electrochemical coating method, the presence of intermetallic particles at the grain boundaries can lead to a nonuniform substrate potential and complicate the coating process [19,20]. TiN-based coatings were deposited in our previous studies by magnetron sputtering [21,22]. TiN coating deposition can significantly increase the Mg-Ca-Zn alloy corrosion resistance. However, it causes substrate heating, resulting in non-uniform coating thickness and phase composition, along with insufficient control of the implant biodegradation. Similar to doping, ion implantation can cause toxic effects of implanted ions during magnesium alloys' biodegradation. While ion implantation of magnesium with Sr and Ti ions increases its corrosion resistance, the biodegradation rate of these alloys has not been studied [23,24]. A promising method for coating magnesium alloys is microarc oxidation (MAO). It does not require careful preparation of the substrate surface and is more economical for protective coating of the implant surface [25]. Coating deposition is performed in a salt solution bath, which prevents local magnesium alloy overheating to obtain a more stable coating with a given biodegradation rate [26]. In addition, MAO is used to form coatings of various chemical compositions depending on the type of electrolyte and processing mode. MAO coatings can effectively increase the corrosion properties of magnesium alloys, and improve biodegradation [27–30]. Antibacterial agents' introduction into the MAO electrolyte can also increase the antibacterial activity of magnesium alloys [10,31].

The structure and properties of MAO coatings depend on the phase and elemental composition of the alloy; therefore, coatings should be primarily studied at the stage of alloy development, which helps optimizing the alloy composition. The choice of optimal parameters for obtaining coatings based on Mg-Ca-Zn alloys will enable biodegradation process control for specific medical applications. Thus, the study of the MAO parameters effects on the structure and properties of coatings based on Mg-Ca-Zn alloys is promising for the creation of medical biodegradable implants with a controlled biodegradation rate.

2. Materials and methods

2.1. Samples and coatings preparation

In this work, Mg-Ca-Zn alloys were produced using 99.99% commercially pure Mg, Ca, and Zn. A total of 1 kg of Mg was placed in a steel crucible, and then melted in an open-type muffle furnace with argon flow to prevent combustion. When the melt temperature reached 720 °C, zinc was introduced in an amount of 1.5 wt%, and then the melt was mechanically stirred at 1200 rpm until its complete dissolution. After reheating the melt to 720 °C, 0.5 wt% calcium was introduced into the melt using a steel bell, and the melt was mechanically stirred for 60 s. The melt was poured into a steel mold placed on the shaker vibrating with a frequency of 60 Hz and an amplitude of 0.5 mm. Vibration treatment of the melt was carried out until complete solidification. More detailed information about the process of melting samples is given in reference [32].

The samples fabricated from the resulting Mg-Ca-Zn alloy were coated in a MAO 10 L stainless steel bath, where electrolyte was mixed via bubbling and coils were used for its cooling. The electrolyte temperature was maintained at 20–25 °C. Cooling was performed using a chiller. A unipolar ARCCOR switch-mode power supply with a power of 6 kW (AO EleSy, Tomsk, Russia) was connected to the MAO bath. The weakly alkaline phosphate-borate electrolyte Manel-W (pH = 8–9) developed and patented by AO MANEL (Russia) was employed for coating with the following composition: up to 50 wt% Na_2HPO_4, up to 40 wt% $Na_2B_4O_7$, and up to 13 wt% NaF. The coating deposition parameters were as follows: 450 V voltage, 150 μs pulse duration, and 50 Hz pulse frequency. These parameters make it possible to obtain stable size pores in the MAO coating [33]. To determine the optimal phase composition and surface properties, the samples were exposed to electrolyte for 5, 10, and 20 min. Table 1 shows the samples designation.

2.2. Surface characterization methods

The microstructure of the cross-section of the coatings synthesized in nitrogen was analyzed with a JEM-2100 transmission electron microscope (TEM) operated at an accelerating voltage of 200 kV using the equipment from the shared use center Nanotech, ISPMS SB RAS. Thin foils were prepared by ion thinning of lamellae cut perpendicular to the coating surface in the cross-section geometry using the EM 09100IS ion slicer (JEOL, Japan). The elemental composition of the coatings was analyzed using an energy-dispersive spectrometer (EDS) in TEM.

The microstructure, surface morphology, and continuity of the coatings were analyzed using the Axia ChemiSEM (Thermo Fisher Scientific, USA) scanning electron microscope (SEM) in conjunction with an elemental composition micro analyzer. The research was carried out using the equipment of the Tomsk Regional Core Shared Research Facilities Center of the National Research Tomsk State University, supported by the grant of the Ministry of Science and Higher Education of the Russian Federation 075-15-2021-693 (No. 13.RFC.21.0012).

Adhesion strength was analyzed by the scratch tests with a load linearly increasing from 0.01 N to 30 N at a loading rate of 30 N/min. The experiment was performed using a Rockwell diamond indenter with a diameter of 100 μm and an indentation rate of 5.25 mm/min.

2.3. Analysis of biodegradation and in vitro/vivo testing

To analyze biodegradation, samples were aseptically immersed in DMPI-1840 synthetic culture medium with a low content of micronutrients (5.9 g/L NaCl, 0.4 g/L KCl, 0.8 g/L $Na_2CO_2O_7$, 0.1 g/L Ca $(CO_3)_2$ $4H_2O$, 0.049 g/L $MgSO_4$, amino acids, and vitamins, Sigma-Aldrich, USA) at 37 °C (1 mL of medium per sample in compliance with ISO 10993-6). Before immersion, all 2 × 10 × 10 mm^3 samples were dry heat sterilized at 453 K for 1 h. The samples were removed after 21 days and air-dried at 22 °C for 14 days to record the changes in the sample weight. The samples were weighed using a BM-II analytical balance with the highest accuracy in compliance with GOST 26104–201 (the standard weight deviation was 0.003–0.009 mg).

MCF-7 cells were used to study the coated alloy surface cytocompatibility. Cells were cultured for 72 h under standard conditions at 37 °C, 5% CO_2, and humidified atmosphere. The complete culture medium consisted of DMEM/F12 (Paneco, RF, Tokyo, Japan) supplemented with 10% fetal bovine serum, 40 μg/mL gentamicin, and 250 mg/L glutamine. Cells were visualized using double staining with acridine orange and ethidium bromide. The surface of the alloys with cells was examined using an LSM-780NLO confocal laser scanning microscope (Carl Zeiss, Jena, Germany). When overlaying fluorescent images,

Table 1
Designation and state of the samples.

Sample	State
M0	Uncoated starting Mg-Ca-Zn alloy
M5	Mg-Ca-Zn alloy after 5 min exposure to electrolyte
M10	Mg-Ca-Zn alloy after 10 min exposure to electrolyte
M20	Mg-Ca-Zn alloy after 20 min exposure to electrolyte

live cells were green, and dead cells were red in the transmitted light.

The experimental study was conducted in the vivarium of the Ural State Medical University, in compliance with the Ethical Guidelines for the Use of Animals in Research and the principles outlined in the European Convention for the Protection of Vertebrate Animals Used for Experimental and Other Scientific Purposes (Strasbourg, France, 1986). The experiments performed to study the coated Mg-Ca-Zn alloy were approved by the local Ethical Committee of the Ural State Medical University, extract from minutes No. 6 dated 17.06.2022. All animals were kept in compliance with sanitary requirements No. 1045-73 of 06.04.1973. The experiment was conducted using 3 mature male laboratory rabbits of the Soviet Chinchilla breed, 1.9–3.1 kg in weight. Cylindrical implants 2 mm in diameter made of the coated Mg-Ca-Zn alloy were implanted in the paws of the animals used in the experiment.

3. Results and discussion

The coating structure was studied by electron microscopic analysis. The analysis of the TEM image showed a dense coating with a gradient structure formed via micro-arc oxidation on the Mg-Ca-Zn alloy surface in Fig. 1. The top layers of the coating are amorphous, as evidenced by a characteristic diffuse halo in the selected area electron diffraction pattern SAED in Fig. 1, Sections 1 and 2. The interface between the amorphous coating layers and the substrate is amorphous-nanocrystalline in Fig. 1, Section 3. The morphology of the layers is visually different. The distinctly contrasting interfaces between the layers indicate the difference in their phase composition.

EDS mapping of the cross-section of thin foils in Fig. 2 identified Mg (30.7 at.%), O (49.6 at.%), P (6.1 at.%), and F (13.6 at.%) elements. The diffusion zone between the substrate and the coating consists mainly of Mg, F, and O elements. The next F-enriched coating layer prevents the diffusion of Mg onto the surface. The upper amorphous coating layer consists of the Mg, O, and P elements. F-enriched inclusions up to 2 μm in size were detected in the amorphous layer.

Alkaline solutions with pH = 12–14 lead to large pores and defects in coating [34,35]. Frequently used silicate and alkaline electrolytes degrade their properties and do not result in repeatable coatings under electrical current or heating. The weakly alkaline phosphate-borate electrolyte with pH = 8–9 used in this work ensured the formation of a multilayer coating with a minimum number of defects in Figs. 1 and 2.

X-ray diffraction patterns of samples M5, M10, and M20 were obtained in the symmetric Bragg-Brentano survey geometry in Fig. 3. From the interpretation of the X-ray spectra, the presence of the Mg phase belonging to the substrate was established. Nonlinear behavior of the diffraction pattern at 20–30° 2θ diffraction angles indicates the presence of amorphous components in the coating. With an increase in the holding time, the value of the amorphous component increases, which indicates an increase in the coating thickness. Presumable coating phases can be P_2O_5, MgO, and MgF_2.

The surface morphology of the coating of the samples M5, M10, and M20 was investigated using SEM and EDS analysis. All the samples exhibit the coating with a porous structure, which is characteristic of micro-arc oxidation and is due to the dielectric breakdown of MAO coating layers in Fig. 4 [36]. As the time of micro-arc oxidation increases, the pore size grows in Fig. 4, which is due to the increased energy of the spark discharge that causes the formation of more rough coatings with larger pores [37]. The porous structure of the coating is most favorable for cell adhesion. The pore space is filled with tissue fluids, connective tissue, young cartilage, and bone tissues to replace bone defects. This reduces the time and improves the quality of implant integration. High-contrast SEM images indicate a high roughness of the sample surface.

The SEM-EDS mapping confirmed the results obtained by TEM-EDS mapping. The coating surface consists mainly of Mg, O, and P elements. Table 2 summarizes the concentrations of surface elements for all the samples. Penetration of electrons into deeper layers of the coating during EDS mapping revealed F-based inclusions. The concentration and size of F-based inclusions decrease with exposure time and the coating thickness. The smallest amount of F was recorded for the sample M20 in Table 2. During micro-arc oxidation, F diffuses from the electrolyte into the coating structure [38], which ultimately decreases its concentration in the electrolyte and the resulting coating.

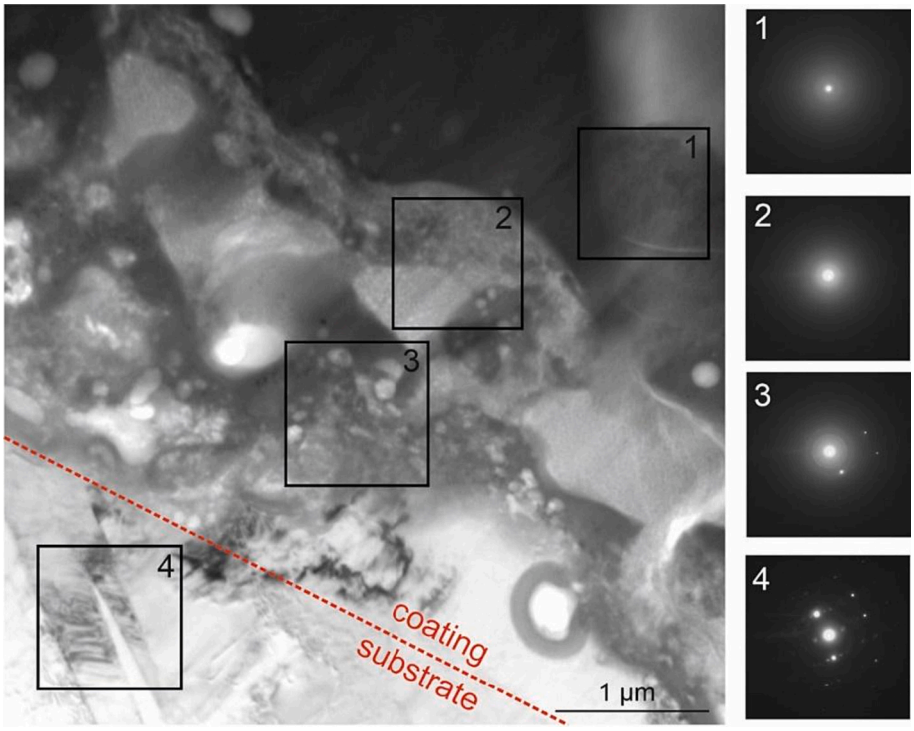

Fig. 1. TEM image of the cross-section of the coating and the selected area electron diffraction patterns of the sample M10, where diffraction patterns 1–3 correspond to areas 1–3 in the TEM image, while diffraction pattern 4 corresponds to the substrate area 4 in the TEM image.

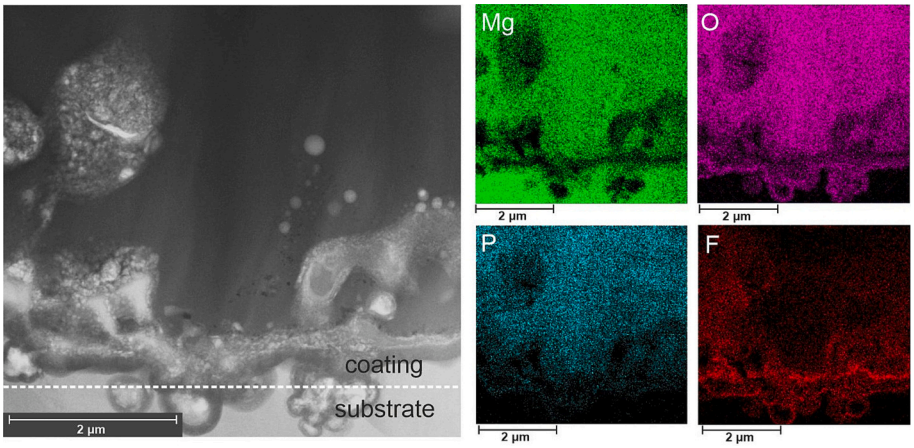

Fig. 2. TEM image of the cross-section of the coating and Mg, O, P, F maps of the sample M10.

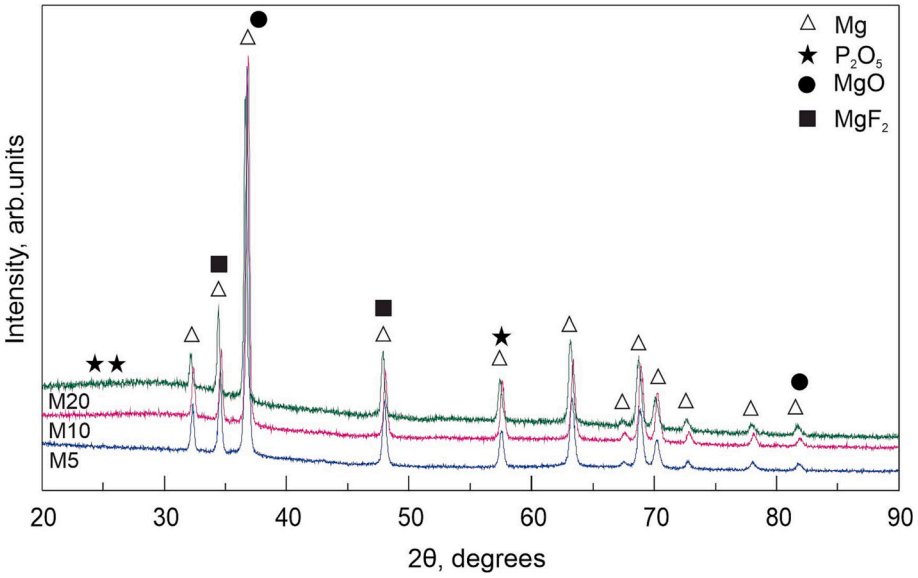

Fig. 3. X-ray diffraction patterns of samples M5, M10, and M20.

The presence of F in the coating has important effects on its properties. Low-fluorine-containing electrolytes lead to MgF_2 deficiency, which degrades coating protection properties and leads to a more rapid onset of corrosion [34,35]. However, high F content of 9–11 at.% limits the formation of preosteoblast and endothelial cells monolayer [39]. The presence of NaF in the electrolyte up to 13 wt% in this work leads to the formation of a dense MgF_2 amorphous nanocrystalline layer, and the F content in the coating does not exceed 5 at.%, which should not harm the cells.

According to the TEM and SEM results, the obtained MAO coating contains Mg, O, F, and P elements, indicating metal and electrolyte components participation in the coating formation. The formation of a multilayer coating on the Mg-Ca-Zn alloy can be described as follows. Initially, an oxide film is formed on the magnesium alloy surface. The spark leads to the discharge channels formation which get filled with electrolyte. A plasma is formed inside these channels, consisting of Mg from the substrate and electrolyte, followed by a plasma-chemical reaction. O ions move towards the substrate, while Mg ions separate from the substrate and move towards the surface, and surface oxides are formed as a result of the reaction between them [40,41]. Anions of fluorides and phosphates released from the electrolyte react with the substrate Mg^{2+} cations in the discharge channels and form a barrier layer in Fig. 2. The hypothetical reactions of the phases appearance in the MAO process are:

$$Mg \rightarrow Mg^{2+} + 2e^- \quad (1)$$

$$2OH^- \rightarrow O^{2-} + H_2O \quad (2)$$

$$NaF \rightarrow Na^+ + F^- \quad (3)$$

$$Mg^{2+} + 2F^- \rightarrow MgF_2 \quad (4)$$

$$Mg^{2+} + O^{2-} \rightarrow MgO \quad (5)$$

$$Mg^{2+} + 2OH^- \rightarrow Mg(OH)_2 \quad (6)$$

$$Mg(OH)_2 \rightarrow MgO + H_2O \quad (7)$$

$$Na_2HPO_4 \leftrightarrow 2Na^+ + HPO_4^{2-} \quad (8)$$

$$HPO_4^{2-} + H_2O \rightarrow H_2PO_4^- + OH^- \quad (9)$$

$$H_2PO_4^- + H_2O \rightarrow H_3PO_4 + OH^- \quad (10)$$

$$2PO_4^{3-} \rightarrow P_2O_5 \quad (11)$$

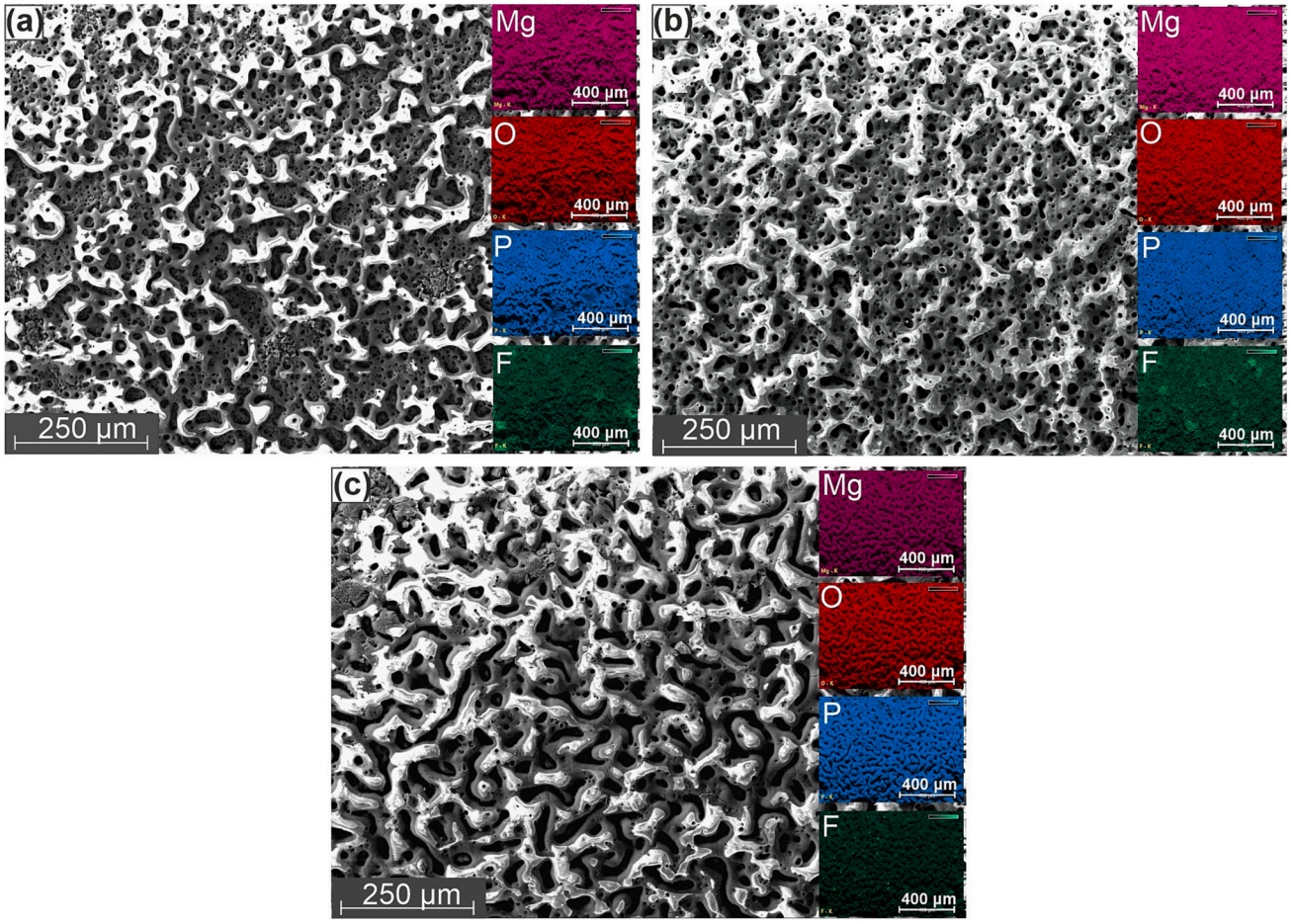

Fig. 4. SEM images of the surface morphology of the coated Mg-Ca-Zn alloy and EDS mapping of the samples (a) M5, (b) M10, and (c) M20.

Table 2
EDS analysis of the Mg-Ca-Zn alloy surfaces coated in electrolyte for different time.

Sample	Element concentration, at.%					
	Mg	O	P	F	Ca	Zn
M5	24.2	63.4	7.5	4.2	0.3	0.4
M10	23.9	65.1	7.7	2.9	0.3	0.2
M20	23.1	67.9	7.7	1.1	0.1	0.1

Table 3
Scratch test for the coatings on Mg-Ca-Zn alloys.

State of the coating	Sample		
	M5	M10	M20
Roughness smoothing	7 N	6 N	5 N
Delamination onset	11 N	12 N	12 N
Complete coating delamination	16 N	18 N	21 N

The coating adhesion strength for Mg-Ca-Zn alloys was studied via scratch tests performed under load linearly increased in the 0.01–30 N range in Fig. 5. Table 3 lists the stress values and the corresponding coating state for all samples. The load at which the coating roughness begins to smooth decreases as the time of sample exposure to electrolyte increases. This is due to the increased overall coating roughness caused by the increased time of sample exposure to electrolytes. The coating thickness increases with exposure time; therefore, complete delamination of the coating for the sample M20 occurs at a higher load in Table 3.

Fig. 5 shows a scratch track on the surface of the M10 sample after

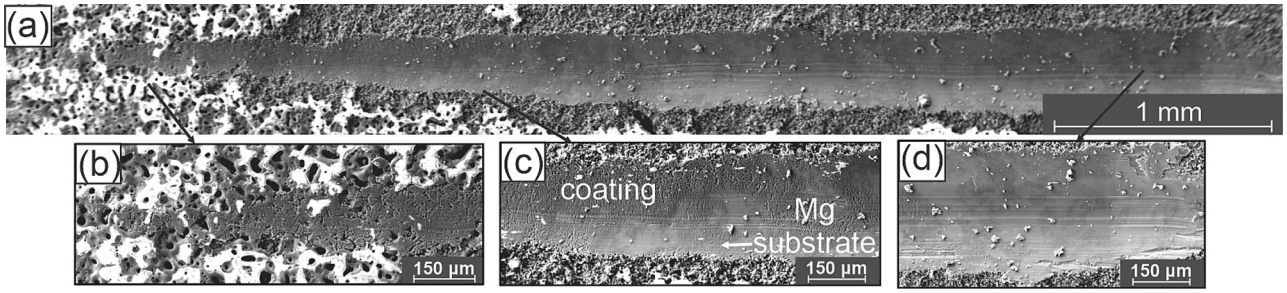

Fig. 5. Scratch test performed for the sample M10: (a) general view of the indenter path, (b) section under 6 N load, (c) section under 12 N load, (d) section under 16 N load.

indentation. When the load is 12 N, the coating begins to break down, which is evidenced by light areas seen on the Mg substrate in Fig. 5(c).

Quantitative measurements of weight loss were performed by immersion of the samples in an aggressive solution to assess the corrosion behavior and biodegradation of alloys. Table 4 shows the values of the initial and final sample weight on day 21 after immersion in the DMPI-1840 culture medium. The weight loss of all the coated Mg-Ca-Zn samples was significantly reduced compared to the uncoated sample. Therefore, the presented method prevents the Mg-Ca-Zn alloys' biodegradation.

Cytocompatibility study using MCF-7 cells is shown in Fig. 6. A large number of pits are observed on the M0 sample surface, which formed during biodegradation after 24 h of cultivation in Fig. 6(a). Active biodegradation of the M0 sample limited the possibility of cell attachment. A denser distribution of cell mass is observed on the surface of the M10 sample in Fig. 6(b).

To study the biocompatibility of coated Mg-Ca-Zn alloys, surgical treatment of the rabbit femur was performed. The study was conducted in sterile conditions under general anesthesia. Intramuscular administration of Zoletil 100 was performed at a dosage of 10 mg/kg of body weight. After pre-cleaning of the surgical area, hair removal, and skin treatment with solutions, a 3 cm skin incision was made along the outer surface of the distal femur on both paws. The distal metaphysis of the femur was isolated by blunt and sharp dissection, and an engraver with a sterile cylindrical tip with a 2 mm diameter was used to make a trephination hole (2 mm × 10 mm) in the distal metaphysis of the femur in Fig. 7(a). After that, the implant of an appropriate diameter was placed in the hole made using tweezers, and it was firmly immersed up to the opposite cortical layer in Fig. 7(b).

The periosteum over the implant was sutured to prevent its migration from the bone. The surgical wound was closed in layers and then treated with brilliant green. The postoperative period was within normal, and the pain was relieved with Flexoprofen 2.5% at a dosage of 2.5 mg/kg of body weight.

Clinical evaluation of the results did not reveal any purulent-inflammatory complications in all animals in the first 28 days after implantation. In the implantation area, palpation was painless, the temperature was not elevated, and the animals showed no movement disorders. Computed tomography (CT) performed on day 28 for all the animals revealed no gas release into soft tissues. Yet, sample M5 exhibited a significant amount of gas in the medullary canal of the femur (up to 1/4 of the entire canal cavity). The implant is poorly contoured in the images, which may be indicative of an active biodegradation stage in Fig. 8(a).

For the M10 sample, CT images of the rabbit femur after implantation show a much smaller amount of gas released into the cavity of the medullary canal in Fig. 8(b). The implant is well-contoured, which may indicate a relatively slow bioresorption. For the M20 sample, CT images of laboratory rabbits obtained after implantation show the least amount of gas in the implantation area in Fig. 8(a). The implant is well-contoured along its entire length.

A 3D simulation of the CT image in airways mode provides a spatial comparison of the amount of gas released in rabbit femurs in Fig. 9. The M20 implant exhibits a negligible amount of gas released compared to the M10 sample implant.

The porous structure of the coating ensures rapid integration of the coated Mg-Ca-Zn implants. Gas evolution decreases with exposure time in the electrolyte and correspondingly with coating thickness. The release of gas in the femur is likely due to the phosphorus concentration. The M20 implant exhibits the lowest phosphorus concentration and the least amount of gas released. At present, a follow-up of the laboratory rabbit condition is underway.

Table 4
Biodegradation of the coated and uncoated Mg-Ca-Zn samples.

Sample	Initial sample weight, g	Sample weight on day 21	Weight loss, g
M0	0.459	0.298	0.16
M5	0.496	0.456	0.04
M10	0.551	0.52	0.03
M20	0.559	0.519	0.04

The results of this work, particularly the biodegradation and biocompatibility studies, show that the tested micro-arc oxidation regimes can be used to produce biocompatible coatings on magnesium alloys. The coated M20 sample showed promise for biomedical applications due to its biocompatibility, mechanical properties, and biodegradation characteristics. It is well known that multiple micropores or high porosity are major drawbacks of MAO coatings for long-term protection or multifunctional surfaces [42,43]. Sealing is a necessary approach to improve the physical barrier role of MAO coatings on Mg alloys. However, the coatings ended up being denser due to the use of a slightly alkaline phosphate-borate electrolyte and the micropore depth on the surface of the coated M20 sample was shallow. The resulting coatings gradually transitioned from a microporous structure to a dense nanocrystalline structure with exposure time, which improves corrosion resistance and provides barrier functions.

The work of other authors also confirms the promising durable and biocompatible MAO coatings on Mg-Ca-Zn alloys for use in medical implants [44–51]. The properties of MAO coatings depend on their microstructure and composition, which are mainly determined by the process and electrolyte parameters. In references [45, 46] the authors showed that MAO coatings on Mg-Ca-Zn alloys improve the corrosion resistance and surface hardness of the alloys. Another study investigated the effects of different electrolyte concentrations on the microstructure and corrosion resistance of MAO coatings on Mg-Ca-Zn alloys and found that higher electrolyte concentrations resulted in better corrosion resistance [47–49]. Researchers have also investigated the possibility of using MAO coatings on Mg-Ca-Zn alloys for bone tissue repair [50,51]. MAO coatings on Mg-Ca-Zn alloys have been shown to improve the mechanical properties, adhesion, and proliferation of bone cells in vitro, making them suitable for use as implants for bone tissue replacement.

4. Conclusions

The coating on the Mg-Ca-Zn alloy was obtained by the MAO method at the electrolyte exposure time of 5, 10, and 20 min. The analysis of the structure, elemental composition, biodegradation, and biocompatibility yielded the following conclusions.

1. As a result of micro-arc oxidation on the surface of the Mg-Ca-Zn alloy, a dense coating with a gradient structure is formed, consisting of amorphous and amorphous-nanocrystalline layers. The amorphous layer mainly consists of O, P, and Mg. Inclusions enriched in F were also found in the amorphous layer. The nanocrystalline layer is enriched in F. The formed layer has a porous structure in all samples, characteristic of micro-arc oxidation with high roughness. As the exposure time in the electrolyte increases, there is a marked decrease in the size and concentration of the inclusions based on F.
2. Scratch testing under load linearly increasing in the 0.01–30 N range revealed good adhesion strength of the coatings. As the electrolyte exposure time increases, the complete coating delamination occurs at a higher load.
3. All the coated Mg-Ca-Zn samples showed a significant reduction in weight loss compared to the uncoated sample on day 21 after immersion in the culture medium. Therefore, the above coating method successfully prevents the biodegradation of Mg-Ca-Zn alloys. Cytocompatibility study using MCF-7 cells showed an increase in the cell mass density on the coated samples.
4. Surgical treatment of the rabbit femurs with the M5, M10, and M20 implants was successful. On day 28 after implantation, no purulent-inflammatory complications were recorded in the animals. Yet, computed tomography showed the presence of gas in the medullary

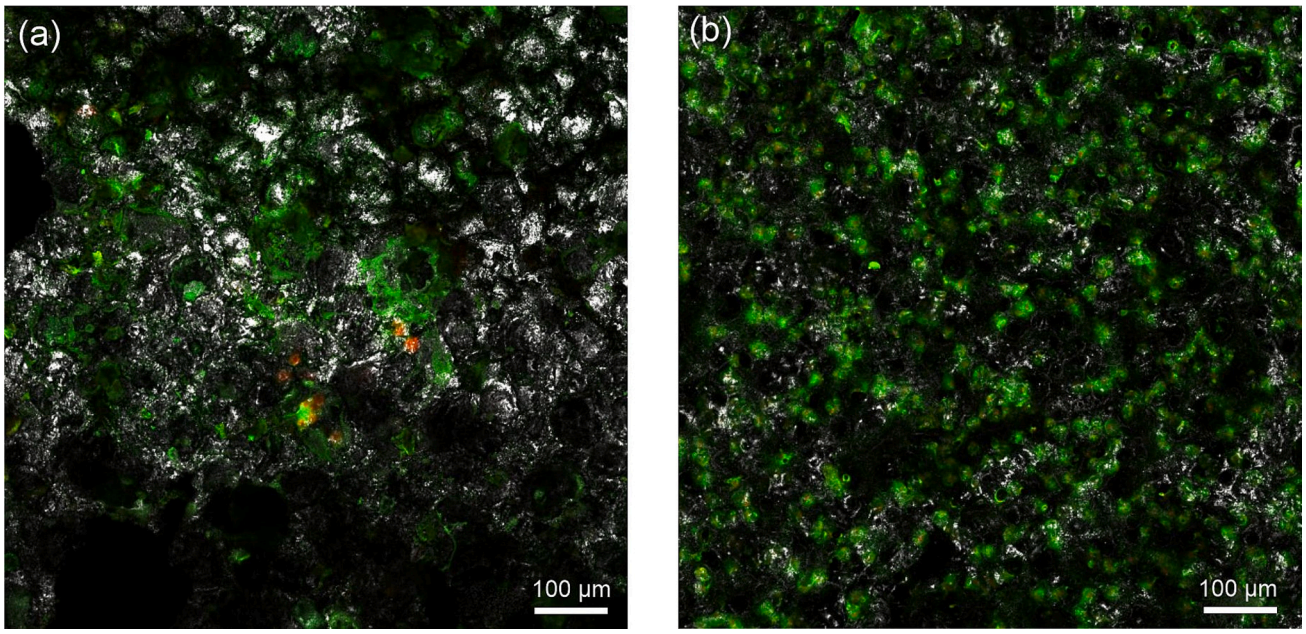

Fig. 6. MCF-7 cells on the surface of (a) M0 and (b) M10 samples.

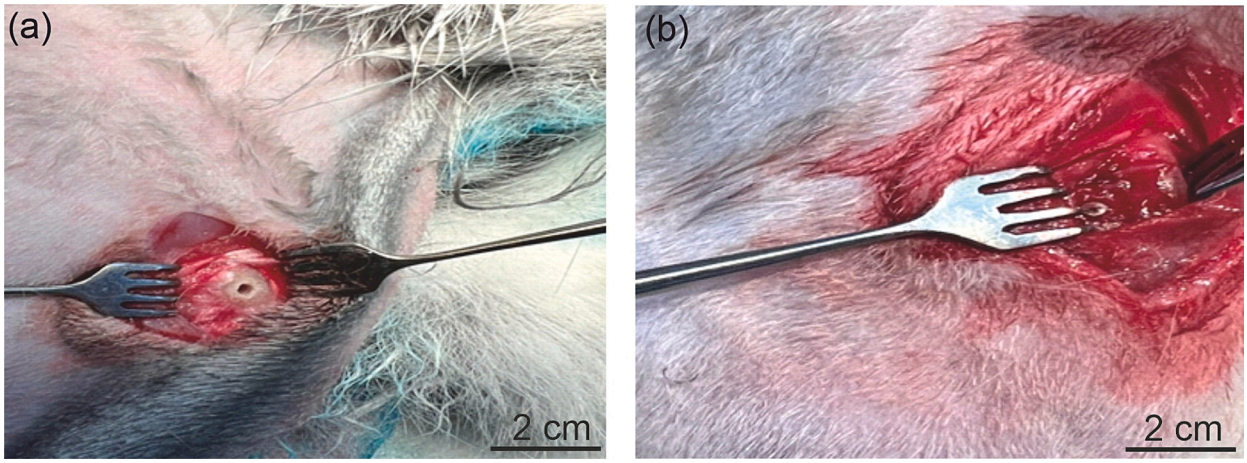

Fig. 7. (a) A 2 mm trephination hole in the distal metaphysis of the femur of the laboratory rabbit; (b) a 2 mm implant placed in the distal metaphysis of the femur of the laboratory rabbit.

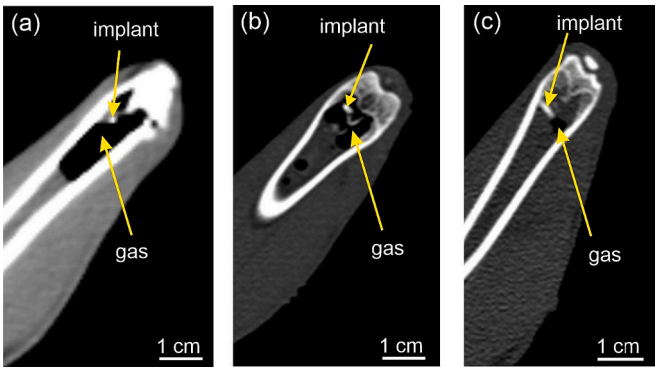

Fig. 8. Frontal CT image of the laboratory rabbits on day 28 after implantation: (a) M5, (b) M10, and (c) M20 implants.

canals of the femurs. The decreased volume of the released gas correlates with the increased time of sample exposure to electrolytes. The thickness of the coating is therefore critical. The release of gas in the femoral bone is probably related to the concentration of fluoride. The M20 implant has the lowest F concentration and the least amount of gas released.

The results of this study have shown the possibility of fabricating Mg-Ca-Zn alloys with a coating that reduces biodegradation and exhibits high biocompatibility. The studies of the implant behavior in the living organism are important in order to perform adjustments of the electrolyte or the alloy composition, which will be conducted in the future.

CRediT authorship contribution statement

Ekaterina S. Marchenko: Writing – review & editing, Supervision, Resources, Project administration, Funding acquisition. **Arina A. Shishelova:** Conceptualization, Investigation, Writing – original draft, Writing – review & editing. **Pavel I. Butyagin:** Methodology, Resources,

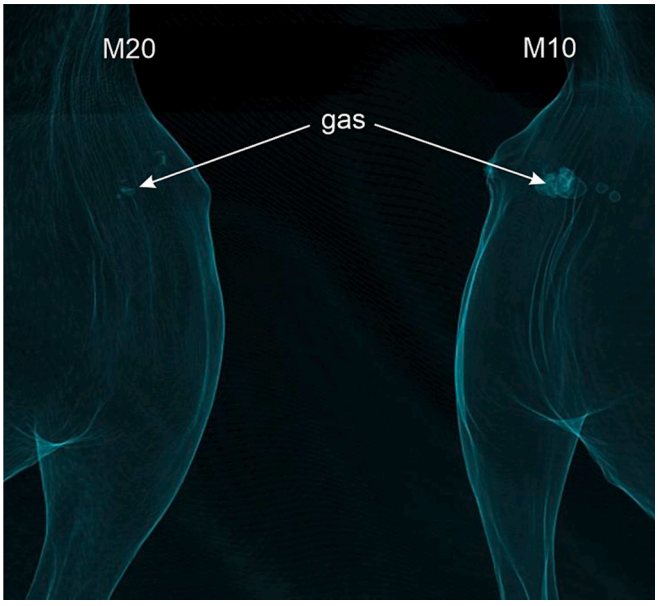

Fig. 9. Frontal section of the 3D model of the CT image of the rabbit femur with the M10 and M20 implants on day 28 after implantation.

Data curation. **Ivan I. Gordienko:** Methodology, Resources, Investigation. **Anton P. Khrustalev:** Conceptualization, Investigation, Formal analysis, Writing – original draft. **Svetlana S. Arbuzova:** Methodology, Resources. **Ilya A. Zhukov:** Validation, Data curation, Formal analysis. **Gulsharat A. Baigonakova:** Conceptualization, Visualization, Writing – review & editing. **Alex A. Volinsky:** Writing – review & editing, Project administration.

Declaration of competing interest

The authors declare that they have no known competing financial interests or personal relationships that could have appeared to influence the work reported in this paper.

Data availability

Data will be made available on request.

Acknowledgments

This research was supported by the Mega grant from the Government of the Russian Federation No. 220 of 9 April 2010 (Agreement No. 075-15-2021-612 of 4 June 2021).

References

[1] Y.F. Zheng, X.N. Gu, F. Witte, Biodegradable metals, Mater. Sci. Eng. R. Rep. 77 (2014) 1–34, https://doi.org/10.1016/j.mser.2014.01.001.
[2] I. Antoniac, M. Miculescu, V. Manescu, A. Stere, P.H. Quan, G. Paltanea, A. Robu, K. Earar, Magnesium-based alloys used in orthopedic surgery, Materials 15 (2022) 1148, https://doi.org/10.3390/ma15031148.
[3] J.L. Wang, J.K. Xu, C. Hopkins, D.H.K. Chow, L. Qin, Biodegradable magnesium-based implants in orthopedics—a general review and perspectives, Adv. Sci. 7 (2020), 1902443, https://doi.org/10.1002/advs.201902443.
[4] V. Tsakiris, C. Tardei, F.M. Clicinschi, Biodegradable Mg alloys for orthopedic implants–a review, J. Magnes. Alloys 9 (2021) 1884–1905, https://doi.org/10.1016/j.jma.2021.06.024.
[5] S. Kumar, P. Katyal, Factors affecting biocompatibility and biodegradation of magnesium based alloys, Mater. Today: Proc. 52 (2022) 1092–1107, https://doi.org/10.1016/j.matpr.2021.10.499.
[6] C. Xu, T. Nakata, G.H. Fan, X.W. Li, G.Z. Tang, S. Kamado, Enhancing strength and creep resistance of Mg-Gd-Y-Zn-Zr alloy by substituting Mn for Zr, J. Magnes. Alloy 7 (2019) 388–399, https://doi.org/10.1016/j.jma.2019.04.007.
[7] Z. Yu, C. Xu, J. Meng, S. Kamado, Microstructure evolution and mechanical properties of a high strength Mg-11.7Gd-4.9Y-0.3Zr (wt%) alloy prepared by pre-deformation annealing, hot extrusion and ageing, Mater. Sci. Eng. A 703 (2017) 348–358, https://doi.org/10.1016/j.msea.2017.06.096.
[8] N. Wang, Y. Ma, H. Shi, Y. Song, S. Guo, S. Yang, Mg-, Zn-, and Fe-based alloys with antibacterial properties as orthopedic implant materials, Front. Bioeng. Biotechnol. 10 (2022), 888084, https://doi.org/10.3389/fbioe.2022.888084.
[9] M. Ali, M.A. Hussein, N. Al-Aqeeli, Magnesium-based composites and alloys for medical applications: a review of mechanical and corrosion properties, J. Alloys Compd. 792 (2019) 1162–1190, https://doi.org/10.1016/j.jallcom.2019.04.080.
[10] A. Fattah-Alhosseini, R. Chaharmahali, K. Babaei, M. Nouri, M.K. Keshvarz, M. Kaseem, A review of effective strides in amelioration of the biocompatibility of PEO coatings on Mg alloys, J. Magnes. Alloy 10 (2022) 2354–2383, https://doi.org/10.1016/j.jma.2022.09.002.
[11] B. Istrate, C. Munteanu, I.V. Antoniac, S.C. Lupescu, Current research studies of Mg–Ca–Zn biodegradable alloys used as orthopedic implants, Crystals 12 (2022) 1468, https://doi.org/10.3390/cryst12101468.
[12] H.R. Bakhsheshi-Rad, M.H. Idris, M.R. Abdul-Kadir, S. Farahany, A. Fereidouni, M. Y. Yahya, Characterization and corrosion behavior of biodegradable Mg-Ca and Mg-Ca-Zn implant alloys, Appl. Mech. Mater. 121–126 (2012) 568–572, https://doi.org/10.4028/www.scientific.net/AMM.121-126.568.
[13] Y. Pan, S. He, D. Wang, D. Huang, T. Zheng, S. Wang, P. Dong, Ch. Chen, In vitro degradation and electrochemical corrosion evaluations of microarc oxidized pure Mg, Mg–Ca and Mg–Ca–Zn alloys for biomedical applications, Mater. Sci. Eng. C. 47 (2015) 85–96, https://doi.org/10.1016/j.msec.2014.11.048.
[14] R. Kumar, P. Katyal, Effects of alloying elements on performance of biodegradable magnesium alloy, Mater. Today: Proc. 56 (2022) 2443–2450, https://doi.org/10.1016/j.matpr.2021.08.233.
[15] T. Kraus, S.F. Fischerauer, A.C. Hänzi, P.J. Uggowitzer, J.F. Löffler, A.M. Weinberg, Magnesium alloys for temporary implants in osteosynthesis: in vivo studies of their degradation and interaction with bone, Acta Biomater. 8 (2012) 1230–1238, https://doi.org/10.1016/j.actbio.2011.11.008.
[16] B. Zhang, Y. Hou, X. Wang, Y. Wang, L. Geng, Mechanical properties, degradation performance and cytotoxicity of Mg–Zn–Ca biomedical alloys with different compositions, Mater. Sci. Eng. C. 31 (2011) 1667–1673, https://doi.org/10.1016/j.msec.2011.07.015.
[17] Y. Jang, Z. Tan, C. Jurey, Z. Xu, Z. Dong, B. Collins, Y. Yun, J. Sankar, Understanding corrosion behavior of Mg–Zn–Ca alloys from subcutaneous mouse model: effect of Zn element concentration and plasma electrolytic oxidation, Mater. Sci. Eng. C 48 (2015) 28–40, https://doi.org/10.1016/j.msec.2014.11.029.
[18] P. Yin, N.F. Li, T. Lei, L. Liu, C. Ouyang, Effects of Ca on microstructure, mechanical and corrosion properties and biocompatibility of Mg–Zn–Ca alloys, J. Mater. Sci. Mater. Med. 24 (2013) 1365–1373, https://doi.org/10.1007/s10856-013-4856-y.
[19] G. Wu, J.M. Ibrahim, P.K. Chu, Surface design of biodegradable magnesium alloys—a review, Surf. Coat. Technol. 233 (2013) 2–12, https://doi.org/10.1016/j.surfcoat.2012.10.009.
[20] J.E. Gray, B. Luan, Protective coatings on magnesium and its alloys—a critical review, J. Alloys Compd. 336 (2002) 88–113, https://doi.org/10.1016/S0925-8388(01)01899-0.
[21] G. Baigonakova, E. Marchenko, I. Zhukov, A. Vorozhtsov, Structure, cytocompatibility and biodegradation of nanocrystalline coated Mg–Ca–Zn alloys, Vacuum. 207 (2023), 111630, https://doi.org/10.1016/j.vacuum.2022.111630.
[22] A. Khrustalyov, A. Monogenov, G. Baigonakova, A. Akhmadieva, E. Marchenko, A. Vorozhtsov, Effect of TiN coating on the structure, mechanical properties and fracture of the Mg-Ca-Zn alloy, Metals 12 (2022) 2140, https://doi.org/10.3390/met12122140.
[23] H. Wu, K. Xi, S. Xiao, A.M. Qasim, R.K. Fu, K. Shi, K. Ding, G. Chen, G. Wu, P. K. Chu, Formation of self-layered hydrothermal coating on magnesium aided by titanium ion implantation: synergistic control of corrosion resistance and cytocompatibility, Surf. Coat. Technol. 401 (2020), 126251, https://doi.org/10.1016/j.surfcoat.2020.126251.
[24] Y. Jia, Z. Ba, Q. Dong, Z. Li, J. Kuang, Surface properties of magnesium improved by Sr ion implantation, Mater. Res. Express 5 (2018), 066546, https://doi.org/10.1088/2053-1591/aacc12.
[25] L. Li, T. Li, Z. Zhang, Z. Chen, C. Chen, F. Chen, Superhydrophobic graphene/hydrophobic polymer coating on a micro-arc oxidized metal surface, J. Coat. Technol. Res. 19 (2022) 1449–1456, https://doi.org/10.1007/s11998-022-00618-w.
[26] W. Yao, L. Wu, J. Wang, B. Jiang, D. Zhang, M. Serdechnova, T. Shulha, C. Blawert, M.L. Zheludkevich, F. Pan, Micro-arc oxidation of magnesium alloys: a review, J. Mater. Sci. Technol. 118 (2022) 158–180, https://doi.org/10.1016/j.jmst.2021.11.053.
[27] M.H. Song, W.J. Yoo, T.J. Cho, Y.K. Park, W.J. Lee, I.H. Choi, In vivo response of growth plate to biodegradable Mg-Ca-Zn alloys depending on the surface modification, Int. J. Mol. Sci. 20 (2019) 3761, https://doi.org/10.3390/ijms20153761.
[28] A. Keyvani, M. Zamani, A. Fattah-Alhosseini, S.H. Nourbakhsh, M. Bahamirian, Microstructure and corrosion resistance of MAO coatings on AZ31 magnesium, Mater. Res. Express 5 (2018), 086510, https://doi.org/10.1088/2053-1591/aad0d4.
[29] Y. Gu, S. Bandopadhyay, C.F. Chen, Y. Guo, C. Ning, Effect of oxidation time on the corrosion behavior of micro-arc oxidation produced AZ31 magnesium alloys in simulated body fluid, J. Alloys Compd. 543 (2012) 109–117, https://doi.org/10.1016/j.jallcom.2012.07.130.
[30] Q. Zeng, S. Chen, P. Song, H. Li, X. Zeng, Enhanced plasticity and corrosion resistance in Mg-Zn-Ca-Cu amorphous alloy composite via plasma electrolytic

oxidation treatment, Metals 12 (2022) 300, https://doi.org/10.3390/met12020300.
[31] A. Fattah-Alhosseini, M. Molaei, M. Nouri, K. Babaei, Antibacterial activity of bioceramic coatings on Mg and its alloys created by plasma electrolytic oxidation (PEO): a review, J. Magnes. Alloy 10 (2022) 81–96, https://doi.org/10.1016/j.jma.2021.05.020.
[32] A.P. Khrustalyov, A. Akhmadieva, A.N. Monogenov, I.A. Zhukov, E.S. Marchenko, A.B. Vorozhtsov, Study of the effect of diamond nanoparticles on the structure and mechanical properties of the medical Mg–Ca–Zn magnesium alloy, Metals 12 (2022) 206, https://doi.org/10.3390/met12020206.
[33] P. Butyagin, S. Arbuzova, A. Kondratenko, A. Bolshanin, Influence of anodic spark mode parameters on the properties of MAO-coatings, in: 7th International Congress on Energy Fluxes and Radiation Effects (EFRE), Tomsk, Russia, 2020, pp. 1164–1168, https://doi.org/10.1109/EFRE47760.2020.9241915.
[34] L. Moreno, M. Mohedano, R. Arrabal, E. Matykina, Development and screening of (Ca-P-Si-F)-PEO coatings for biodegradability control of Mg-Zn-Ca alloys, J. Magnes. Alloy 10 (2022) 2220–2237, https://doi.org/10.1016/j.jma.2021.12.011.
[35] L. Fu, Y. Yang, L. Zhang, Y. Wu, J. Liang, B. Cao, Preparation and characterization of fluoride-incorporated plasma electrolytic oxidation coatings on the AZ31 magnesium alloy, Coatings 9 (2019) (2019) 826, https://doi.org/10.3390/coatings9120826.
[36] L. Zhang, J. Zhang, C.F. Chen, Y. Gu, Advances in microarc oxidation coated AZ31 Mg alloys for biomedical applications, Corros. Sci. 91 (2015) 7–28, https://doi.org/10.1016/j.corsci.2014.11.001.
[37] T.S. Narayanan, I.S. Park, M.H. Lee, Strategies to improve the corrosion resistance of micro-arc oxidation (MAO) coated magnesium alloys for degradable implants: prospects and challenges, Prog. Mater. Sci. 60 (2014) 1–71, https://doi.org/10.1016/j.pmatsci.2013.08.002.
[38] J. Liang, B. Guo, J. Tian, H. Liu, J. Zhou, T. Xu, Effect of potassium fluoride in electrolytic solution on the structure and properties of microarc oxidation coatings on magnesium alloy, Appl. Surf. Sci. 252 (2005) 345–351, https://doi.org/10.1016/j.apsusc.2005.01.007.
[39] A. Santos-Coquillat, M. Esteban-Lucia, E. Martinez-Campos, M. Mohedano, R. Arrabal, C. Blawert, M.L. Zheludkevich, E. Matykina, PEO coatings design for Mg-Ca alloy for cardiovascular stent and bone regeneration applications, Mater. Sci. Eng. C 105 (2019), 110026, https://doi.org/10.1016/j.msec.2019.110026.
[40] Z. Lin, T. Wang, X. Yu, X. Sun, H. Yang, Functionalization treatment of micro-arc oxidation coatings on magnesium alloys: a review, J. Alloys Compd. 879 (2021), 160453, https://doi.org/10.1016/j.jallcom.2021.160453.
[41] B.L. Jiang, Y.F., Ge Micro-arc oxidation (MAO) to improve the corrosion resistance of magnesium (Mg) alloys, in: G. Song (Ed.), Corrosion Prevention of Magnesium Alloys, Woodhead Publishing, Sawston, 2013, pp. 163–196, https://doi.org/10.1533/9780857098962.2.163.
[42] X.P. Lu, M. Mohedano, C. Blawert, E. Matykina, R. Arrabal, K. Kainer, M. L. Zheludkevich, Plasma electrolytic oxidation coatings with particle additions – a review, Surf. Coat. Technol. 307 (2016) 1165–1182, https://doi.org/10.1016/j.surfcoat.2016.08.055.
[43] U. Malayoglu, K.C. Tekin, S. Shrestha, Influence of post-treatment on the corrosion resistance of PEO coated AM50B and AM60B Mg alloys, Surf. Coat. Technol. 205 (2010) 1793–1798, https://doi.org/10.1016/j.surfcoat.2010.08.022.
[44] T.O. Olugbade, B.O. Omiyale, O.T. Ojo, Corrosion, corrosion fatigue, and protection of magnesium alloys: mechanisms, measurements, and mitigation, J. Mater. Eng. Perform. 31 (2022) 1707–1727, https://doi.org/10.1007/s11665-021-06355-2.
[45] X.N. Gu, N. Li, W.R. Zhou, Y.F. Zheng, X. Zhao, Q.Z. Cai, L. Ruan, Corrosion resistance and surface biocompatibility of a microarc oxidation coating on a Mg-Ca alloy, Acta Biomater. 7 (2011) 1880–1889, https://doi.org/10.1016/j.actbio.2010.11.034.
[46] Z.Z. Yin, W.C. Qi, R.C. Zeng, X.B. Chen, C.D. Gu, S.K. Guan, Y.F. Zheng, Advances in coatings on biodegradable magnesium alloys, J. Magnes. Alloys 8 (1) (2020) 42–65, https://doi.org/10.1016/j.jma.2019.09.008.
[47] Z.Y. Ding, L.Y. Cui, X.B. Chen, R.Ch. Zeng, S.K. Guan, S.Q. Li, F. Zhang, Y.H. Zou, Q.Y. Liu, In vitro corrosion of micro-arc oxidation coating on Mg-1Li-1Ca alloy — the influence of intermetallic compound Mg2Ca, J. Alloys Compd. 764 (5) (2018) 250–260, https://doi.org/10.1016/j.jallcom.2018.06.073.
[48] Y. Chen, J. Dou, Z. Pang, H. Yu, C. Chen, J. Feng, Improving the corrosion resistance of micro-arc oxidation coated Mg–Zn–Ca alloy, RSC Adv. 10 (2020) 8244–8254, https://doi.org/10.1039/C9RA10741J.
[49] Y. Wang, M. Chen, Y. Zhao, Preparation and corrosion resistance of microarc oxidation-coated biomedical Mg-Zn-Ca alloy in the silicon-phosphorus-mixed electrolyte, ACS Omega 4 (2019) 20937–20947, https://doi.org/10.1021/acsomega.9b01998.
[50] P. Tong, Y. Sheng, R. Hou, M. Iqbal, L. Chen, J. Li, Recent progress on coatings of biomedical magnesium alloy, Smart Mater. Med. 3 (2022) 104–116, https://doi.org/10.1016/j.smaim.2021.12.007.
[51] A. Jana, M. Das, V.K. Balla, In vitro and in vivo degradation assessment and preventive measures of biodegradable Mg alloys for biomedical applications, J. Biomed. Mater. Res. A 110 (2) (2022) 462–487, https://doi.org/10.1002/jbm.a.37297.